forests

MDPI

Article

Influence of Cell Characteristics on the Construction of Structural Color Layers on Wood Surfaces

Jing Hu [1,2], Yi Liu [1,2] and Wei Xu [1,2,*]

[1] College of Furnishings and Industrial Design, Nanjing Forestry University, Nanjing 210037, China; hujingnanlin@njfu.edu.cn (J.H.); liuyi@njfu.edu.cn (Y.L.)
[2] Jiangsu Co-Innovation Center of Efficient Processing and Utilization of Forest Resources, Nanjing 210037, China
* Correspondence: xuwei@njfu.edu.cn; Tel.: +86-025-85427528

Abstract: When utilizing microspheres to construct structural color layers on wood surfaces, the cellular structure of wood can influence the self-assembly of microspheres and the resulting structural color layers. To investigate this influence, seven types of wood were selected in this study, and structural color layers were constructed on their surfaces. A comparative analysis was conducted on the color production and macro and micro morphologies of the structural color layers on different wood surfaces, along with an examination of the types and causes of surface defects. The study found that when a microsphere-containing emulsion was applied to a wood surface, the emulsion tended to flow along the vessels of hardwood and the tracheids of softwood. Overflow or seepage of the emulsion could lead to a reduction in the number of microspheres per unit area, resulting in uneven thickness and uneven color generation of the structural color layers. Although the structural color layers on different wood exhibited the same color, there were variations in their tones, appearance, and morphology. Defects such as minor bumps and pits were present on the structural color layers. Bump defects might originate from microsphere encapsulation of fiber bundles or the displacement of air within vessel lumens by emulsion, while pits were mainly caused by the inflow of emulsion into the vessel lumens. This study clarified the influence of wood surface cells, particularly vessels and tracheids, on the construction and color production of structural color layers, providing support for the controllable modification of wood surfaces using structural colors.

Keywords: structural color layer; wood surface; cell characteristics; vessel; defect

check for updates

Citation: Hu, J.; Liu, Y.; Xu, W. Influence of Cell Characteristics on the Construction of Structural Color Layers on Wood Surfaces. *Forests* **2024**, *15*, 676. https://doi.org/10.3390/f15040676

Academic Editor: Boštjan Lesar

Received: 19 March 2024
Revised: 3 April 2024
Accepted: 8 April 2024
Published: 9 April 2024

Copyright: © 2024 by the authors. Licensee MDPI, Basel, Switzerland. This article is an open access article distributed under the terms and conditions of the Creative Commons Attribution (CC BY) license (https://creativecommons.org/licenses/by/4.0/).

1. Introduction

Wood, as a natural material with renewable and sustainable advantages, finds widespread applications in various environments ranging from indoor furniture to outdoor architecture [1,2]. Nowadays, drastic changes in the climate and environment have raised awareness of the importance of natural ecosystems, particularly forest ecosystems with a vast biomass, necessitating the protection and sustainable and efficient utilization of forests [3,4]. Currently, the Chinese timber market is flooded with low-quality wood, characterized by its pale color and ordinary grain, which often requires color modification before being transformed into consumer products [5,6]. Artificially constructing a structural color layer on the surface of wood represents a novel color modification strategy [7]. Unlike the color-producing mechanism of dyes, structural color arises from the interference, diffraction, or refraction of light by ordered microstructures [8].

Utilizing microspheres as the fundamental building blocks, the ordered construction of photonic crystals on the wooden surface generates structural colors that exhibit a captivating iridescent effect. This color modification technique is reminiscent of ancient Chinese methods of furniture decoration, specifically the mother-of-pear inlay, where natural structural colors derived from conch shells, mussel shells, and other materials were skillfully

integrated into the wood surface to create decorative patterns [9]. The structural color modification technology offers a unique and innovative approach to enhancing the visual appeal of wooden products. It not only endows low-grade, light-colored wood with vibrant and brilliant hues, but also ensures the long-term stability of these colors. Specifically, this technique boasts the advantage of color retention, making it resistant to fading over time [10].

The utilization of the self-assembly method of microspheres serves as an effective approach for constructing a structural color layer on wood surfaces. This technique boasts remarkable advantages, including simplicity in processing equipment and low manufacturing costs [11]. During the self-assembly process, microspheres with surface charges, uniformly dispersed in a liquid medium, spontaneously aggregate under the influence of various forces such as evaporation of the dispersing medium. This aggregation aims to achieve the minimum free energy of the system, ultimately leading to the formation of an ordered arrangement of photonic crystal structures [12–14].

Previous studies had demonstrated that thermally assisted gravity deposition could facilitate the complete and orderly self-assembly of microspheres on the wooden surface, enabling structural color decoration [7]. By fine-tuning the particle size of the microspheres, the lattice parameters of the photonic crystals could be modulated, conferring diverse colors to the structural color layer [15]. It was noteworthy that the nature of the wood substrate could significantly influence the self-assembly process of microspheres. However, there is currently a lack of research outcomes that systematically delve into the mechanisms of how wood influences the construction and color generation on its surface structural color layer.

Distinct from synthetic materials, such as glass, metal, and plastic, which possess dense and smooth surfaces, wood is a natural, porous polymeric material composed of diverse cellular structures [16,17]. Furthermore, wood exhibits a complex organizational structure, with coniferous wood primarily consisting of axial tracheids and ray parenchyma cells, while broadleaf wood comprises vessels, wood fibers, axial parenchyma, and transverse ray cells, among others [18]. The cellular dimensions and specific microstructural features of wood vary significantly between species. In practical applications, the surface of wood often presents a large number of cut cells, whether in cross, radial, or tangential sections [19]. Consequently, the wood surface exhibits a microscopic morphology characterized by micrometer-scale roughness and a multicavity pore nature, encompassing both cell cavities and walls.

Therefore, it is imperative to investigate the relationship between the cellular structure of wood and the formation of structural color layers on its surface. In this study, seven commonly available wood species, exhibiting light hues and distinct vessels or tracheids attributes, were chosen to fabricate structural color layers on their surfaces through thermally assisted gravity deposition. By comparing the structural color layers obtained from diverse wood surfaces under identical conditions, we aimed to delve into the disparities in the flatness and color-generating capabilities of these layers, which are influenced by the species of wood and their primary cellular attributes. Furthermore, we endeavored to explain the impact of cellular structure of wood on the assembly of emulsions and microspheres.

Through this study, we can clarify the essential factors of the cellular characteristics of wood, as the substrate for structural color construction, that affect the structural color layer formation and color production, thereby providing a theoretical foundation for promoting the application of structural color modification technology in wood and the wood products industry.

2. Materials and Methods

2.1. Materials and Woods

In this study, all chemicals utilized were of analytical purity (AR) and were directly utilized without any additional purification steps. The styrene (St) monomer was procured

from Shanghai Macklin Biochemical Technology Co. (Shanghai, China). Furthermore, ammonium persulfate (APS) and sodium dodecylbenzene sulfonate (SDBS) were sourced from Shanghai Lingfeng Chemical Reagent Co. (Shanghai, China), whereas ethanol was obtained from Nanjing Chemical Reagent Co. (Nanjing, China). The water used in the experiments was ultrapure, prepared within our laboratory using a Plus-E3 ultrapure water dispenser (18.2 MΩ·cm, Nanjing EPED Co., Ltd. (Nanjing, China)).

To delve into the impact of wood cell characteristics on structural color layer formation, this study selected seven woods: quaking aspen (QA, *Populus tremuloides* Michx.), yellow poplar (YP, *Liriodendron tulipifera* L.), hard maple (HM, *Acer saccharum* Marshall), white birch (WB, *Betula platyphylla* Suk.), manchurian walnut (MW, *Juglans mandshurica* Maxim.), manchurian ash (MA, *Fraxinus mandshurica* Rupr.), and scotch pine (SP, *Pinus sylvestris* Linn. var. *mongolica* Litv.). Sources for these woods included Alberta, Canada for QA, Taobao shop North American Lumber Retail East China for YP, Taobao shop Woodworker Prince Handcrafted Playwood Wood for HM and MW, Taobao shop Hongsheng Wood 62 for WB, Nanjing Lumber Market for MA, and Taobao shop Green Pine Wood for SP. All woods had an air-dry moisture content of approximately 6%.

The selection of these seven types of wood is based on several criteria. Firstly, these timbers are known for their lighter hues and are widely used in interior and exterior decoration. Secondly, the seven timbers include six broadleaf and one coniferous timber, representing two typical types of timber. Crucially, the choice of these six broadleaf timbers builds upon previous research [20] and exhibits variations in type, number, cell diameter, and smoothness of vessels, offering a degree of representativeness. Additionally, the selection encompasses woods with diverse anatomical structures and cell diameters, fulfilling our research objective of investigating the impact of wood surface cell characteristics on the formation of structural color layers.

2.2. Synthesis of Emulsion Containing PSt Microsphere

Emulsions containing polystyrene (PSt) microsphere were successfully synthesized using emulsion polymerization with water and ethanol as dispersing media, following the polymerization process outlined in prior studies [21]. APS served as the initiator, while SDBS functioned as the emulsifier; both were dissolved in a 5:2 mixture of water and ethanol. This mixture was stirred at 400 rpm and heated to 75 °C using an overhead mixer. Subsequently, the St monomer was introduced, and the reaction was allowed to proceed for 6 h, ultimately yielding a PSt emulsion with a solid content of 14.7%.

To assess the microscopic morphology of the structural color layer and PSt microspheres, scanning electron microscopy (SEM) was employed. Utilizing ImageJ software (version 1.52a), the diameters of over 300 microspheres within the SEM images were accurately measured. The resulting data revealed an average particle size of 207.4 nm, accompanied by a low coefficient of variation of 0.028. This excellent monodispersity ensures that the PSt microspheres are well suited for the construction of ordered photonic crystal structures.

2.3. Construction of Structural Color Layers on the Wood Surface

Seven wood specimens were uniformly sawn to dimensions of 4 cm × 4 cm × 1 cm. The impact of the cut surface and fiber angle on the wood surface morphology was disregarded, mirroring its practical application where the specimens' larger surfaces exhibited radial tangential cuts. Prior research has established that certain woods, after being treated with 400 grit sandpaper, can achieve relatively smooth and suitable surfaces for the construction of structural color layers [20]. To eliminate any variations arising from grinding, all seven wood types underwent the same grinding treatment using 400 grit sandpaper. Subsequently, compressed air was used to blow away any residual wood dust adhering to the surface. A 3 cm × 3 cm wireframe was gently outlined on the wood surface using a pencil. Within this wireframe, 40.8 μL/cm^2 of the PSt microsphere-containing emulsion was evenly drop-coated. The coated specimens were then transferred to a 50 °C drying oven for thermally

assisted gravity deposition self-assembly. The drying time was set to 1 h to ensure complete evaporation of the dispersing medium.

2.4. Characterization

A Nikon D7000 digital camera (Nikon Imaging (China) Sales Co., Ltd., Shanghai, China) was utilized to capture the surfaces of seven types of wood after grinding and the structural color layers formed using the emulsion. To record the colored appearance of the structural color layer, the light source was positioned perpendicular to the specimen, with the camera aligned at a 0° angle to the light source. Conversely, a 30° angle was adopted to capture the non-colored appearance.

In this study, digital photos captured at 0° angle between the camera and the light source were analyzed to investigate the colors presented by structural color layers on different wood surfaces. The structural color layer areas in the photos were divided into 25 segments, and the average chromaticity values, expressed as CIE $L^*a^*b^*$ tristimulus values [22,23], were measured for each segment using the straw tool in Photoshop (version 25.4.0). Subsequently, the Convert color data tool on the EasyRGB (http://www.easyrgb.com/en/, accessed on 3 April 2024) was employed to recreate the tristimulus values as theoretical colors, simulating a 2° observer angle under D65 standard illuminants. Utilizing these replicated theoretical colors, seven composite images were assembled, which collectively portrayed and enabled a comprehensive evaluation of the color exhibited by the structural color layers on the wood surfaces. The reason for not directly using a colorimeter to obtain the tristimulus values is due to the coloring mechanism of structural colors and the limitations of the colorimeter. When the test head of the colorimeter is covered on the surface of the structural color layer, the light emitted by its light source cannot directly irradiate the surface of the structural color layer. This occlusion disrupts the interaction between the light and the microstructure, leading to inaccurate and potentially misleading data.

Furthermore, an environmental scanning electron microscope (Prisma E, Thermo Fisher Scientific-CN, Shanghai, China) was utilized to characterize the surface and cross-sectional morphology of the structural color layers on seven wood surfaces, aiming to elucidate the migration and distribution of microspheres within the cellular cavities of the wood surface. Cut the wood samples with structural color layers into samples with volumes of 10 × 10 × 2 mm and 10 × 2 × 2 mm, respectively, for observing the surface and cross-sectional morphology of the structural color layers. After a 100 s gold spray treatment, the microstructure of the samples was photographed.

3. Results and Discussion

3.1. Differences in the Appearance of Structural Color Layers Constructed on the Surfaces of Various Woods

The PSt microsphere emulsion was uniformly drop-coated onto the surfaces of various wood species to fabricate structural color layers under identical conditions of concentration, drop-loading volume, and self-assembly, as depicted in Figure 1, and more complete and clear images were shown in the Supporting Information, as shown in Figures S1–S7. Notably, the surface morphologies of different woods exhibited distinct variations, leading to disparities in the appearance of the structural color layers. Generally, these structural color layers shared certain common characteristics. For instance, the blue-green hue effectively obscured the original wood surface, rendering the grain and natural coloring of the wood indistinct, thus fulfilling the objective of altering the wood's coloration. Furthermore, the surface of the structural color layer was not entirely smooth and flat, exhibiting noticeable cracks and imperfections.

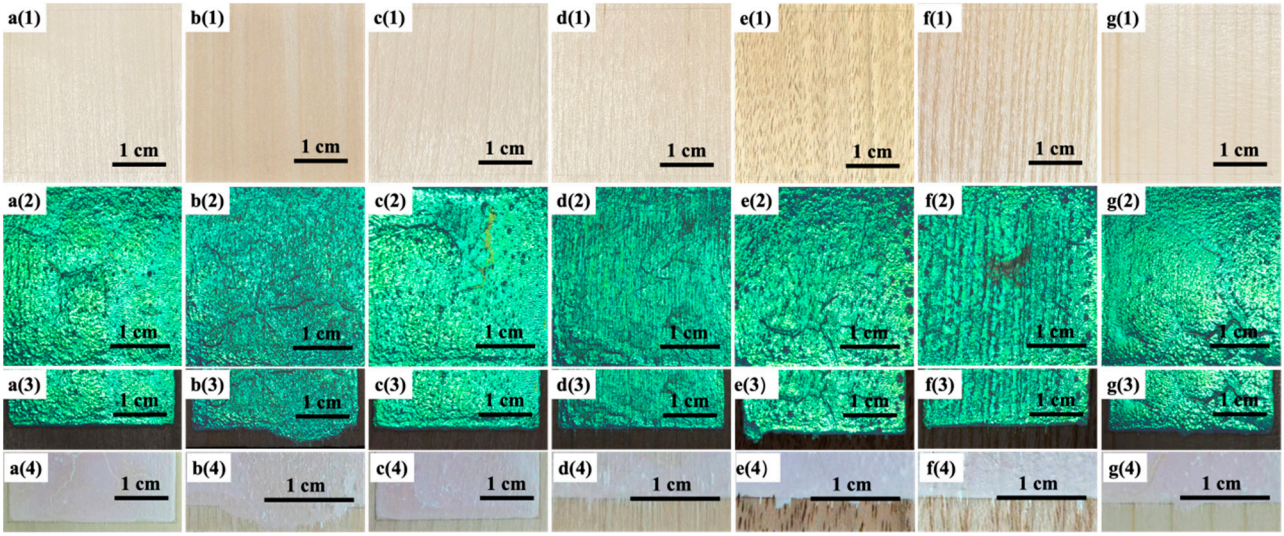

Figure 1. Macroscopic photographs of seven types of wood and their surface structural color layers: (**a**) QA; (**b**) YP; (**c**) HM; (**d**) WB; (**e**) MW; (**f**) MA; (**g**) SP; (**1**) wood surface; (**2**) structural color layers on wood surface at 0° angle between the light source and the camera; (**3**) localization of structural color layers at 0° angle; and (**4**) localization of structural color layers at 30° angle.

Crack defects within the structural color layer arose during the emulsion evaporation drying and microsphere self-assembly process. These defects were linked to the dynamics of microsphere self-assembly. Once the emulsion droplets were applied to the wood surface, thermally assisted gravitational deposition was initiated. As the solvent evaporated, a portion of the microspheres migrated towards the liquid surface, gradually arranging into an orderly, closely packed structure. Simultaneously, another portion of the microspheres, influenced by gravity and the wood's water-absorbing quality, accumulated in a disordered manner on the wood's uneven surface. Due to the spreading nature of emulsions, drying initiated at the liquid's peripheral edges, where the emulsion layer was thinnest and evaporation occurred most rapidly. As the dispersant evaporated, microspheres were drawn towards the edges of the emulsion's surface, initiating the self-assembly process from the edges and progressing towards the center. This phenomenon was commonly known as the coffee ring effect, which occurred during the emulsion drying process [24]. Throughout the drying process, the photonic crystal structure of the liquid surface underwent continuous motion, rather than remaining static after assembly. This motion was influenced by numerous directional forces and ultimately stabilized as the surrounding solvent evaporated. As the emulsion solvent evaporated from the periphery towards the center, the microspheres continued to experience the pulling force caused by evaporation at the edges. This resulted in the microspheres accumulating around and above the edges, creating a tensile situation that ultimately led to the formation of macroscopic crack defects. Furthermore, due to the variability of wood substrates, the final evaporation locations of the emulsion varied, leading to no discernible regularity in the area of the crack defects observed on the structural color layers of the seven types of wood.

In addition to the aforementioned common characteristics, there existed notable differences in the structural color layers deposited on the surfaces of various woods. Although the structural color layers in the photograph exhibit a general blue-green hue, it is noteworthy that their specific tones vary significantly. In order to gain a more nuanced understanding of these color differences, this study employed computer software to extract the CIE Lab tristimulus values of the colors present in distinct areas of the photographs. Subsequently, these tristimulus values were used to recreate color blocks, which were then assembled to form theoretical images of the structural color layers, as illustrated in Figure 2. The images indeed provide a vivid and detailed representation of the structural color layer's uneven color tone. To assess color differences among various structural color layers, this study

conducted a statistical analysis by averaging the L^*, a^*, and b^* values of 25 color blocks for each layer. The obtained results are shown in Table 1. It can be seen that a more uniform dark-green coloration was exhibited on YP, WB, and MA from Figure 2. The structural color brightness of the other four types of wood surfaces was higher (QA, HM, MW, and SP), with a higher L^* value and a slightly higher b^* value, indicating a slightly yellowish green color tone, as shown in Table 1.

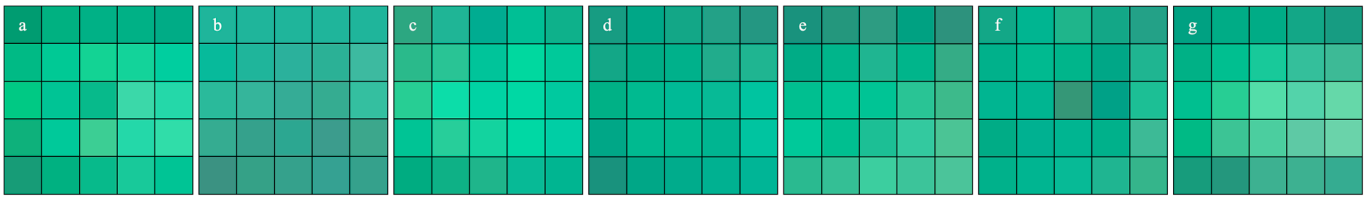

Figure 2. Simulated coating color block images based on L^*, a^*, and b^* values of wood surface structural color layers; (**a**) QA; (**b**) YP; (**c**) HM; (**d**) WB; (**e**) MW; (**f**) MA; and (**g**) SP.

Table 1. The average $L^*a^*b^*$ color values of the surface structural color layers of different woods.

Wood	L^*	a^*	b^*
QA	72.09	−35.89	15.51
YP	66.13	−26.8	4.97
HM	72.87	−35.27	13.44
WB	65.92	−31.52	9.36
MW	69.13	−31.94	12.35
MA	66.76	−31.42	10.02
SP	70.24	−31.43	12.07

Except for chromatic parameters, the cellular structure and grain pattern of the woods, corresponding to its original surface morphology, exerted an influence on certain structural color layers. For instance, traces of the wood's texture were faintly discernible on the structural color layers deposited on YP, WB, MW, and MA, as illustrated in Figure 1b(2),d(2),e(2),f(2). Similarly, a subtle wood texture was also visible on the surface of the structural color layer on HM, particularly in the upper portion of the image, as seen in Figure 1c(2). Upon close inspection of the edge of the structural color layers, it became evident that for several of the aforementioned timbers, there was a noticeable degree of emulsion spilling out of the wireframe at the periphery of the structural color layers. Furthermore, these overflows occurred preferentially along the direction of the wood grain, manifesting as visible traces on the upper and lower sides, while remaining absent on the left and right sides. Additionally, the shape of the overflow varied; while YP exhibited a large overflow followed by a sharp linear protrusion, all other timbers (WB, MW, and MA) displayed a sharp linear overflow pattern that aligned with the wireframe and coincided with the growth direction of the vessels. Given that the vessels serve as the primary water-conducting structures in hardwood, it could be reasonably inferred that these conduits served as the primary channels for emulsion overflow on the surface of these woods. YP wood has a smaller vessel size but a larger tissue ratio, while WB, MW, and MA wood have larger vessel sizes.

On MW and MA, which possessed medium and large vessel diameters, it was clearly evident that the emulsion overflowed predominantly along the vessels. Within these vessels, the microspheres underwent orderly self-assembly, resulting in the exhibition of vibrant structural colors, as depicted in Figure 1e(3),f(3). However, on WB, due to the smaller size than MW, MA and smoother internal structure of its vessels, the emulsion traveled along them and emerged from the ends without successfully forming an ordered

structure. Consequently, most of the overflows lacked distinct coloring and exhibited white filaments, as seen in Figure 1d(3).

In fact, during the testing phase, it was observed that the ends of WB exhibited emulsion spillage, and HM was also encompassed, as exhibited in Figure 3. For WB, the emulsion spillage primarily occurred along the timber surface, flowing downward to form a continuous sheet. However, there were also instances of discontinuous spillage spots. Conversely, for HM, the emulsion ooze was less prominent in terms of surface overflow and continuous flow. Instead, it appeared as discrete point-like ooze directly. Based on these observations, it could be inferred that the vessels served as the primary channels for both surface emulsion overflow and internal ooze.

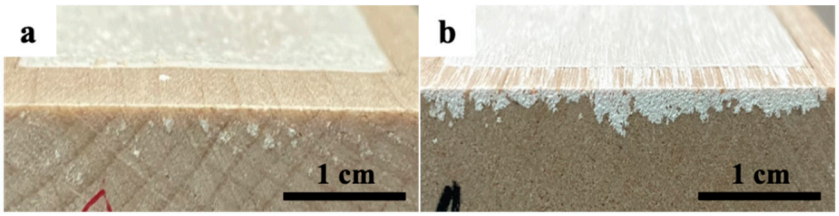

Figure 3. Emulsion spillage on HM and WB ends: (**a**) HM; and (**b**) WB.

The phenomenon that was observed, where the structural color layers on the surfaces of YP, WB, MW, MA, and certain regions of HM retained the original wood texture, could be attributed to several factors. Firstly, the microsphere-containing emulsion might have filled the grooves present in the surface vessels, similar to the situation when constructing structural color layers on the surface of fabrics [14,25]. Secondly, the emulsion might have overflowed along the path of the vessels. Both of these occurrences led to a decrease in the number of microspheres within a specified area, resulting in the formation of a thinner structural color layer. Consequently, the texture of the underlying substrate wood became more apparent.

Upon close examination of the structural color layer on SP surface, depicted in Figure 1g(3,4), it was evident that the layer remained intact, with no exposure of the underlying substrate texture. However, traces of emulsion overflows, similar to those observed in WB, were visible in the edge areas, manifesting as white streaks. Notably, these overflows were primarily concentrated in the earlywood region. Unlike WB, the overflow route on the surface of SP was significantly shorter, failing to reach the wood's terminus, and there was no end overflow. This suggested that the emulsion overflow was minimal and did not compromise the structural color layer's integrity. Furthermore, it could be inferred that the tracheids of the coniferous timber served as the primary channel for emulsion overflow.

Prior research had established that the microscopic irregularities of the wood surface significantly impacted the formation and color production of the structural color layer. Notably, when the abrasive belt grit used for grinding the surface of the treated wood exceeded 320 grit, the inherent structural characteristics of the wood emerged as the primary influencing factor [20]. In the case of broadleaf timber, the vessels represented the cells with the largest radial diameter and water-conducting function, whereas in coniferous timber, these functions were fulfilled by tracheids [26]. Consequently, it was evident that the primary cells present in the surface layer of wood exerted a profound influence on emulsion transportation and drying, microspheres assembly and formation, as well as the color and morphology of the structural color layer.

3.2. The Impact of Wood Surface Cells on the Microscopic Morphology of Structural Color Layers

The macroscopic morphological variations observed in structured color layers were linked to their microscopic morphology. These microscopic morphological differences primarily stemmed from structural disparities in the self-assembly configuration of microspheres. Given that the PSt microsphere-containing emulsion and the self-assembly

environmental conditions remained consistent throughout this study, the primary source of variation in the structural color layers could be attributed to the woods. To explore the influence of the wood surface's microscopic uneven cell structure on microsphere assemblies, SEM analysis was employed to characterize both the surface and cross-section of the structural color layers across seven distinct wood surfaces. This analysis particularly focused on elucidating the effects exerted by cellular structures such as vessels and tracheids.

As depicted in Figure 4, the surface and cross-sectional morphology of the structural color layers exhibited common characteristics across different wood surfaces. In the high-magnification surface images, Figure 4a(2)–g(2), ordered regions were observed within the structural color layers of various wood surfaces. These regions comprised microspheres arranged in a close-packed manner, resembling structural color layers formed by microspheres on other base materials [27,28]. During the self-assembly process, microspheres initially coalesced on the emulsion surface and assembled into numerous lamellar photonic crystals. Subsequently, these lamellae aggregated to form structural color layers. Since the shape and size of the lamellae were random, they could not be seamlessly interconnected, resulting in irregular microscopic linear defects [7].

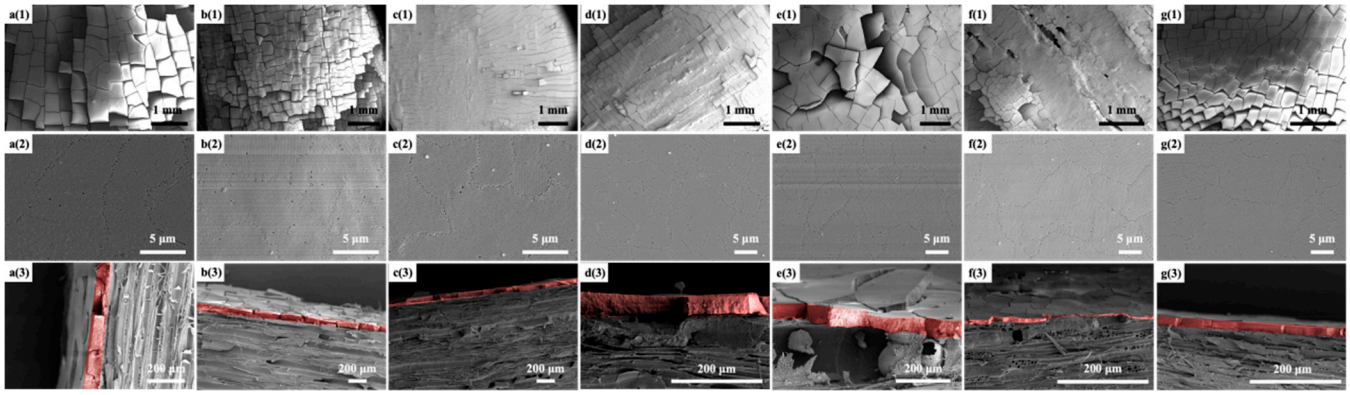

Figure 4. Surface and cross-sectional micromorphology of structural color layers on the surface of seven wood species: (**a**) QA; (**b**) YP; (**c**) HM; (**d**) WB; (**e**) MW; (**f**) MA; (**g**) SP; (**1**) surface low magnification; (**2**) surface high magnification; and (**3**) cross-section low magnification; the red represents the vertical section of the structural color layer.

In the low-magnification surface images, such as Figure 4a(1)–g(1), the structural color layers on the wood surfaces appeared fragmented into numerous small pieces. This fragmentation can be attributed to two primary factors. Firstly, during the preparation of electron microscope specimens, it was necessary to divide the larger wood samples into smaller pieces suitable for microscopy. The handling and manipulation of the woods during this process led to the shattering and cracking of the surface structural color layers. Secondly, as the emulsion dried to its final stage, drying stress was generated, causing the connections between the microspheres to break, resulting in the formation of fragments. This was an inevitable outcome of the transition of the emulsion from its liquid phase to a solid state [29]. Currently, scholars are investigating and attempting to construct structural color layers without cracks [30], or to obtain regularly distributed cracks by regulating the self-assembly process [31,32].

In the cross-sectional views, as presented in Figure 4a(3)–g(3), the lateral morphologies of the structural color layers adhered to the wood surfaces were evident, with the red areas indicating cross-sections of these layers. Notably, these cross-sections resulted from the tearing of the woods rather than slicing with a knife. As observed in the figures, the structural color layers exhibited varying degrees of microscopic irregularity, which was attributed to the diverse anatomical characteristics of the woods. Particularly, MW and MA exhibited the most significant undulations in their surface structural color layers. This was due to their large diameter of vessels, which allowed for the emulsion to infiltrate

into the vessel grooves, creating concavities. Consequently, it was evident that there must have been significant thickness variations in the structural color layers across different wood types.

3.3. Relationship between the Morphology of Structural Color Layer Defects and Wood Surface Cells

Defects within the structural color layers on the surface of wood significantly impacted the layer's levelling effect and were closely linked to the substrates provided by the wood's cells and tissues. As observed in Figures 1 and 4, defects such as micro-bulges, pits, and bleed-throughs in the structural color layers of wood surfaces led to inconsistencies in color generating. To elucidate the specific characteristics of structural color layers on diverse wood surfaces, we selected and highlighted the primary defects present on various surfaces, as depicted in Figure 5. It should be pointed out that this set of pictures is not to illustrate that there is only one type of defect on the surface of a certain wood, but to show the possible types of defects that may occur.

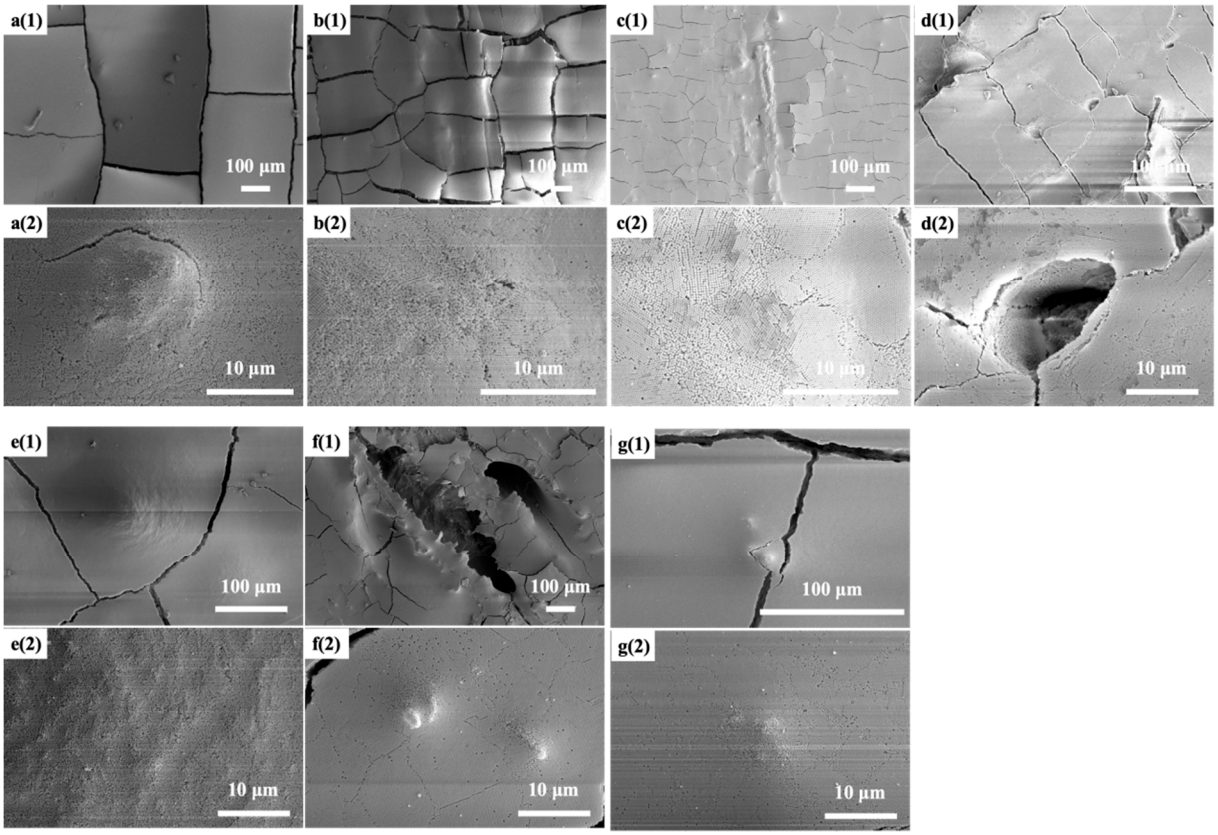

Figure 5. Surface defects of structural color layers constructed on seven types of wood: (**a**) QA; (**b**) YP; (**c**) HM; (**d**) WB; (**e**) MW; (**f**) MA; (**g**) SP; (**1**) low magnification image; and (**2**) high magnification image.

Raised and depressed defects occurred on the surface of every type of wood, but the state of these defects varied depending on various factors. For instance, point-like bulges, resembling gentle hills composed of stacked microspheres, retained their ordered arrangement in the surrounding planar region upon magnification of the surface structure. However, the long-range ordered structure was disrupted in the hill portion, as observed in Figure 5a(2),e(1),f(2),g(1,2). This kind of defect appeared as a small dot in macroscopic photographs, which can be distributed in any corner of the structural color layers. Wavy bulges, or surface unevenness of the structural color layers, were evident on the surfaces of YP, HM, and MW, as depicted in Figure 5b(1,2),c(1,2),e(2). These regions exhibited a mix of ordered and disordered arrangements of surface microspheres. Notably, woods with

larger vessel diameters exhibited prominent concave defects, as shown in Figure 5d(1,2),f(1). These holes and grooves contained traces of microsphere infiltration and accumulation, forming a continuous structure that interconnected with the microspheres in the outer flat portion.

The longitudinal section view of the structural color layers also revealed the presence of defects, as depicted in Figure 6. Here, two distinct cases of the formation of point-like bulge defects were observed. Figure 6a(1,2) shows a dot-like bulge on the surface of QA, arising from a rod-like fiber bundle measuring approximately 170 μm in length and 11 μm in width. This fiber bundle attracted a significant number of microspheres, which converged and wrapped around it, creating a bulging structure thicker in the middle and thinner on the sides. The fiber bundle was likely cell walls that were pulled and lifted when cut by abrasive grains on the sandpaper surface, resulting in a relative displacement with the wood during the grinding process. A closer inspection, as seen in Figure 6a(2), revealed that the surface of the fiber bundle was generally wrapped in a disordered arrangement of microspheres. This suggested that the wrapping of the fiber bundle by the microspheres occurred simultaneously in different regions, ultimately forming multiple blocks, as indicated by the yellow and green regions in the figure. The emergence of this form was potentially linked to the process of fiber bundle deformation. Initially, the fiber bundles, formed through grinding, adhered to the wood surface in a flattened state. Upon the application of emulsion droplets, the fiber bundles commenced to absorb water, leading to deformation and erection. Subsequently, microspheres began to cluster around the fiber bundle as the focal point. Concurrently, microspheres aggregated and deposited in other areas of the wood surface, ultimately intersecting with the clusters surrounding the fiber bundle. This phenomenon could be observed on the surfaces of various tree species, as the wood surface inherently contained numerous fiber bundles. However, the mechanical properties of wood cells varied, and the size and length of fiber bundles formed after grinding with sandpaper differed, resulting in variations in the size of the resulting point-like bulges.

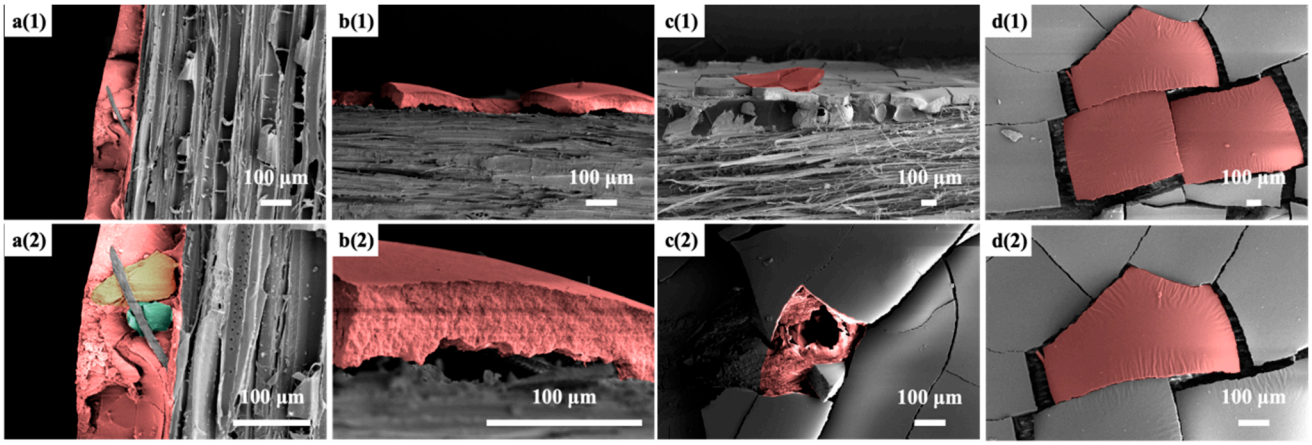

Figure 6. Dot bulging defects on the structural color layer of the wood surface: (**a**) QA; (**b**) HM; (**c**) MW; (**d**) MA; (**1**) low-magnification SEM image; (**2**) high-magnification SEM image; the red represents the bulging structural color layer; and the green and yellow are used to highlight the microspheres surrounding the fiber bundles to form a disordered layer in different regions.

Furthermore, another type of pitting bulge defect arose due to the emulsion penetrating the interior of the wood. As depicted in Figure 6b(1,2), the punctate bulge on the HM surface, devoid of wrapped fiber bundles, exhibited a hollow bulge phenomenon, with no contact with the wood surface and no accumulation of microspheres within. In Figure 6b(2), the high-magnification SEM image clearly revealed this bulge structure, where the thickness of the structural color layer remained uniform, unlike the aforementioned QA, which exhibited thickness variations. On the surface of MA, as seen in Figure 6d(1,2), the

red area stood out in a distinctly elevated state, detached from the surrounding plates. The formation of these detached slabs occurred during the initial construction of the structural color layer, rather than being the result of later splitting caused by the impact of the wood knocking during the preparation of SEM test specimens.

This was evident in Figure 6d(1), where clear traces of folding were visible around the edges of all three raised red areas. Such traces could only be formed during the self-assembly of microspheres to construct the structural color layer. It was possible that, during the self-assembly process, a continuous piecewise ordered structure was initially formed on the emulsion surface layer but was then subjected to an upward force between the substrate and the emulsion generated by air displacement, causing the surface layer to enter a tensile state. As the emulsion dispersion medium evaporated, the microspheres and structural color layers dried out, preserving their morphological structure. The upward force responsible for this structure likely originated from trapped air within the vessel. When the emulsion covered the vessel cavity, the air within was not smoothly displaced, resulting in air bubbles remaining during the construction of the structural color layer, ultimately shaping its form. If the fractured plates were the result of later impacts during sample preparation, there would have been no folds adjacent to the fractures atop the bulge, and the flat areas surrounding the fractures would have remained unfolded. Furthermore, the cracks around the bulge highlighted its mechanical fragility, a weakness inherent in the structure constructed by microspheres. Notably, these initially formed fragments, whether due to island formation or violent shocks during sampling, and remained adhered to the wood surface, indicating that some microspheres maintained a connection with the wood substrate at their base.

On the surface of MW, a bulging phenomenon was also observed, as exemplified by the red area in Figure 6c(1). In contrast, Figure 6c(2) revealed a substrate hole or vessel cavity where the structural color layer had been lost. This contrasted with Figure 5d(2), where traces of microsphere ooze were evident from the hole defect, indicating no residual microspheres. This suggested that air within the hole had exerted a repulsive force against the microsphere emulsion. Considering the fracture patterns of the adjacent structural color layer, it was conceivable that the original structural color layer here may have exhibited a bulging structure akin to that in Figure 6d but had been detached from the defect due to external forces. Comparing the hole sizes in Figure 5d(2) and Figure 6c(2), the former measured approximately 20 μm in length, while the latter measured approximately 156 μm. Notably, the larger holes did not exhibit emulsion overflow, implying that the formation of bulging structures was associated with the smoothness of air replacement within the catheter lumen. This smoothness was indicative of the catheter's functional performance. If the catheter was smooth, air could be effectively expelled through other ports, facilitating the flow of emulsion through the lumen. Conversely, if the catheter was not smooth, pressure differences within the lumen could lead to the formation of bulges.

The primary cause of various defects in the structural color layer, including uneven thickness, bulging, pits, and grooves, was attributed to the overflow and seepage of the emulsion on the wood surface, leading to a reduction in the number of microspheres per unit area. As demonstrated in Figures 7 and 8, these images showcased the microscopic morphology of the emulsion overflow and seepage phenomena observed during the construction of the structural color layers on the wood surface. For this study, four types of wood were selected: YP, WB, MA, and SP. When compared to the macroscopic morphology presented in Figure 1, it was evident that the phenomenon of emulsion overflow along the wood surface was present in all these wood types. The micro-morphological images corroborated the previous analysis. As shown in Figure 7, after applying the emulsion droplets to the wood surface, the primary surface overflow channels were vessels and tracheids. The cutting process left a significant number of exposed conduits and tubular cavities on the wood surface.

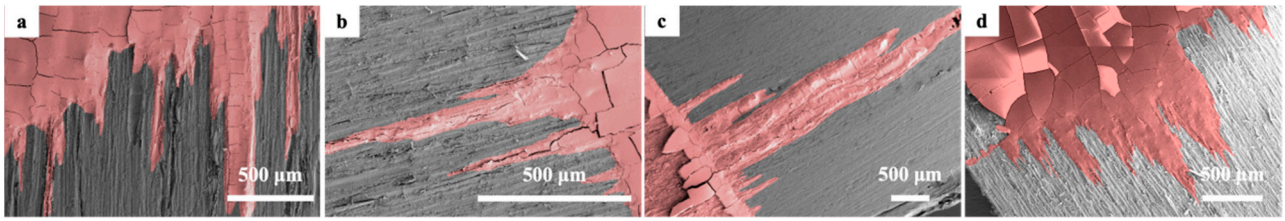

Figure 7. Overflow phenomenon of emulsion at the edges of the structural color layer on the surface of four types of wood: (**a**) YP; (**b**) WB; (**c**) MA; and (**d**) SP. The red areas represent the structural color layer.

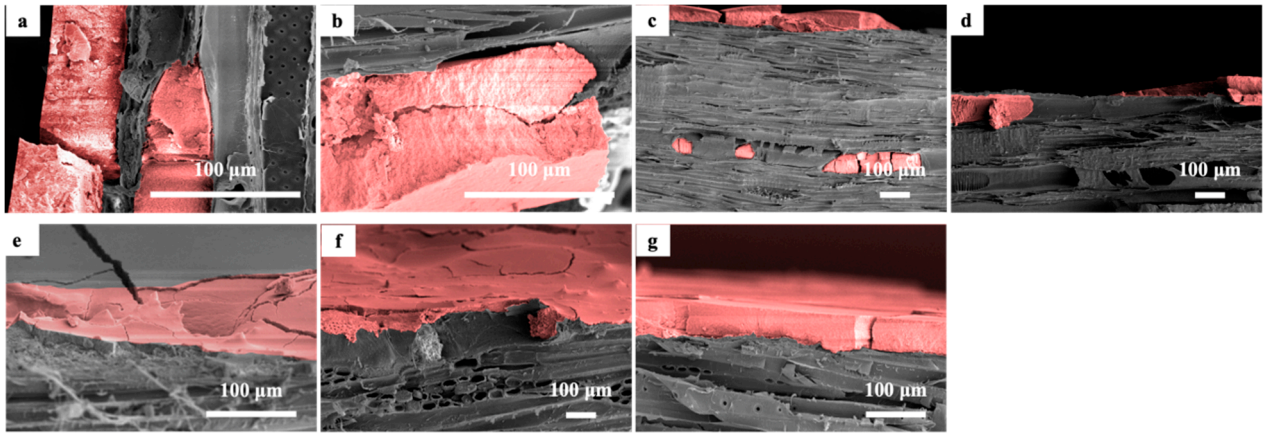

Figure 8. Overflow and infiltration phenomena observed in the longitudinal profiles of structural color layers constructed on seven different types of wood: (**a**) QA; (**b**) YP; (**c**) HM; (**d**) WB; (**e**) MW; (**f**) MA; and (**g**) SP. The red color is used to highlight the presence of the structural color layer and microspheres within the conduit cavity.

When the emulsion droplet was applied, it spread across the wood surface and filled these vessels and tracheids. When the emulsion reached the edges of the wireframe, the presence of emulsion tension created a certain degree of edge resistance, thereby preventing the emulsion from overflowing excessively. However, the wettability of the emulsion to the wood surface was intricately linked to the nature of the wood [33]. The varying vessel sizes and distribution patterns across different wood surfaces served as crucial factors influencing emulsion overflow. Notably, YP exhibited a more severe overflow compared to WB and MA. This was primarily attributed to the higher density of vessels per unit area on the surface of YP, resulting in the formation of more grooves (YP 107.7/mm^2, WB 43.5/mm^2, MA 9.8/mm^2). On the other hand, the overflow channels on the surface of SP were primarily tracheids, which possessed a smaller diameter compared to vessels. Although the number of tracheids was higher within a unit area, the overflow pattern of the emulsion on the surface of SP was comparable to that of YP. However, the amount of overflow was less, and the distance traversed was shorter.

Observation of longitudinal SEM images of the structural color layers on the surfaces of seven wood species revealed that the emulsion penetrated and flowed into the interior of the wood along the cut cells, as depicted in Figure 8. Beneath the surface layers of QA, WB, and MA, microspheres were observed having flowed into and filling the cavities within adjacent vessels, as shown in Figure 8a,d,f. Notably, there were distinct differences in the conditions exhibited by these three species. In the side view of the structural color layer on the surface of QA, as seen in Figure 8a, the openings for emulsion flow into the vessel were not evident, potentially due to limitations in the sampling length. Figure 8d presents a side view of WB, with the sampling location at the edge of the finish. The red area on the right represented the structural color layer within the wireframe, exhibiting a clear thinning trend in thickness. No traces of microsphere overflow were observed in the vessel

cavity directly beneath it. However, the red area on the left was clearly situated below the wood surface, indicating that microspheres had entered through an overflow of the vessel cavity somewhere exposed on the wood surface. In the side view of MA, as shown in Figure 8f, microspheres flowing into the vessel cavity were clearly visible. Figure 8e, a longitudinal section of MW, illustrates the lateral view of emulsion having flowed into the vessel opening.

The side view of HM revealed a distinct emulsion transport phenomenon compared to the previously mentioned woods, as evident in Figure 8c. Within the HM, traces of microsphere assembly were observed in the vessel, situated further away from the wood's surface. This observation corroborated the existence of hard maple end surfaces that had lacked direct connection to the surface but instead exhibited punctate overflow traces on their ends, as shown in Figure 3. The vessel distribution in HM differed significantly from that of the aforementioned species, primarily due to the presence of multiple rows of shaped wood rays. The vessels grew around these rays, adopting a curved shape. In the processed surface layer of HM, there were exposed vessel cavities that had facilitated the emulsion's entry into the cavities and subsequent traversal along the curved path into the wood. This process had resulted in localized unevenness within the structural color layer on the HM. Additionally, the replacement of air with emulsion in the vessel cavities often led to the formation of hollow pitting defects.

Figure 8b,g presented a side view of YP, revealing microspheres densely packed and assembled within the exposed vessel cavity on the wood's surface. The thickness of the structural color layer in this region measured approximately 78.8 μm, which exceeded the average thickness observed on the surface of YP. This variance in thickness between the vessel cavity and non-vessel areas accounted for the irregular appearance of the structural color layer on the YP, as exemplified in Figure 1b(2). In contrast, when considering SP, the emulsion failed to penetrate the sub-surface and deeper layers of the wood within the tracheids, as depicted in Figure 8g. Instead, only a minimal amount spilled over along the tracheids at the surface. This limited transport was presumably due to the smaller diameter of the tracheids and their inferior transport capacity compared to that of the vessels.

4. Conclusions

Based on the above analysis of the surface and cross-sectional micromorphology of the structural color layers on different wood surfaces, the following conclusions can be drawn.

1. The cell structure of wood and surface processing traces can have impacts on the self-assembly of microspheres and the structural color layers.
2. Microspheres have a sub-micrometer scale, while the maximum micro-roughness of wood can reach tens of micrometers, representing a significant gap of two orders of magnitude between the two. Therefore, when we constructed a structural color layer on the surface of wood, a sufficient number of microspheres were required to fill the surface grooves and self-assemble into an ordered structure.
3. Microspheres dispersed in the emulsion, in a flowable state, could overflow and infiltrate along the main liquid transport channels on the surface of the wood. Among them, the main channels for liquid transportation in hardwood are vessels, while in softwood, they are tracheids.
4. The diameter and patency of vessels and tracheids can directly affect the construction of the structural color layer. When the diameter of the vessels was large, such as in MW and MA, the emulsion surrounding the vessels could flow into the vessels, resulting in concave defects in the structural color layer. When the interior of the vessels was relatively unobstructed, such as in YP, HM, WB, etc., the emulsion could be transported along the vessels, causing surface overflow or internal infiltration, which resulted in a decrease in the thickness and unevenness in the flatness of the structural color layers.
5. Based on the conclusions mentioned, to ensure the structural color layers possess the desired and uniform thickness and surface homogeneity, there are two main

approaches. Firstly, selecting wood with smaller cell size and a uniform structure is crucial. Secondly, for woods with larger cells and an unobstructed internal structure, it is recommended to use putty and pig blood ash to fill holes prior to applying the emulsion. This step is similar to traditional wood finishing techniques and ensures that the surface is smooth and ready to receive the color layer.

Supplementary Materials: The following supporting information can be downloaded at: https://www.mdpi.com/article/10.3390/f15040676/s1, Figure S1. The original wood and structural color layers on QA. Figure S2. The original wood and structural color layers on YP. Figure S3. The original wood and structural color layers on HM. Figure S4. The original wood and structural color layers on WB. Figure S5. The original wood and structural color layers on MW. Figure S6. The original wood and structural color layers on MA. Figure S7. The original wood and structural color layers on SP.

Author Contributions: Conceptualization, J.H., Y.L. and W.X.; methodology, J.H. and Y.L.; data curation, J.H.; writing—original draft preparation, J.H.; writing—review and editing, J.H.; visualization, J.H. All authors have read and agreed to the published version of the manuscript.

Funding: This research was funded by Natural Science Foundation of Jiangsu Province (grant number BK20230403, Jiangsu Provincial Department of Science and Technology); Postgraduate Research & Practice Innovation Program of Jiangsu Province (grant number KYCX23_1196, Jiangsu Education Department); Qing Lan Project (Jiangsu Education Department).

Data Availability Statement: The raw and processed data required to reproduce these findings cannot be shared at this time as the data also forms part of an ongoing study.

Acknowledgments: The authors acknowledge the valuable support from Nanjing Forestry University.

Conflicts of Interest: The authors declare no conflicts of interest.

References

1. Fu, Y.; Zhang, Y.; Wang, Y. Improvement of flame-retardant and antistatic property of wood using a spray-assisted layer-by-layer self-assembly technique. *Wood Mater. Sci. Eng.* **2023**, *18*, 1553–1561. [CrossRef]
2. Chen, M.; Zhang, H.; Wu, Y. Improving the decorative performance of UV-curable coatings with iridescent cellulose nanocrystal film. *RSC Adv.* **2023**, *13*, 22569–22578. [CrossRef] [PubMed]
3. Chambers, J.Q.; Tribuzy, E.S.; Toledo, L.C.; Crispim, B.F.; Higuchi, N.; dos Santos, J.; Araújo, A.C.; Kruijt, B.; Nobre, A.D.; Trumbore, S.E. Respiration from a tropical forest ecosystem: Partitioning of sources and low carbon use efficiency. *Ecol. Appl.* **2004**, *14*, 72–88. [CrossRef]
4. Ji, Y.; Zhou, G.; Luo, T.; Dan, Y.; Zhou, L.; Lv, X. Variation of net primary productivity and its drivers in China's forests during 2000–2018. *For. Ecosyst.* **2020**, *7*, 15. [CrossRef]
5. Qi, Y.; Sun, Y.; Zhou, Z.; Huang, Y.; Li, J.; Liu, G. Response surface optimization based on freeze-thaw cycle pretreatment of poplar wood dyeing effect. *Wood Res.* **2023**, *68*, 293–305. [CrossRef]
6. Yu, Y.; Yan, K.; Ramaswamy, H.S.; Zhu, S.; Li, H.; Hu, L.; Jiang, X. Dyeing of poplar wood through high-pressure processing: Performance evaluation. *Trans. ASABE* **2019**, *62*, 1163–1171. [CrossRef]
7. Liu, Y. Self-assembly of poly(styrene-methyl methacrylate-acrylic acid) (P(St-MMA-AA)) colloidal microspheres on wood surface by thermal-assisted gravity deposition. *Wood Sci. Technol.* **2021**, *55*, 403–417. [CrossRef]
8. Kinoshita, S.; Yoshioka, S.; Miyazaki, J. Physics of structural colors. *Rep. Prog. Phys.* **2008**, *71*, 076401. [CrossRef]
9. Yu, J.; Bai, P. Application exploration of mother-of-pearl inlay technology in fashion furniture design. *Furniture* **2020**, *41*, 62–65. [CrossRef]
10. He, Y.; Liu, L.; Fu, Q.; Ge, J. Precise assembly of highly crystalline colloidal photonic crystals inside the polyester yarns: A spray coating synthesis for breathable and durable fabrics with saturated structural colors. *Adv. Funct. Mater.* **2022**, *32*, 076401. [CrossRef]
11. von Freymann, G.; Kitaev, V.; Lotsch, B.V.; Ozin, G.A. Bottom-up assembly of photonic crystals. *Chem. Soc. Rev.* **2013**, *42*, 2528–2554. [CrossRef] [PubMed]
12. Li, Z.; Wang, J.; Song, Y. Self-assembly of latex particles for colloidal crystals. *Particuology* **2011**, *9*, 559–565. [CrossRef]
13. Gao, W.; Rigout, M.; Owens, H. Self-assembly of silica colloidal crystal thin films with tuneable structural colours over a wide visible spectrum. *Appl. Surf. Sci.* **2016**, *380*, 12–15. [CrossRef]
14. Li, Y.; Zhou, L.; Zhang, G.; Liu, G.; Fan, Q.; Shao, J. Study on the effects of the characteristics of textile substrates on the photonic crystal films and the related structural colors. *Surf. Coat. Technol.* **2017**, *319*, 267–276. [CrossRef]
15. Goerlitzer, E.S.A.; Taylor, R.N.K.; Vogel, N. Bioinspired photonic pigments from colloidal self-assembly. *Adv. Mater.* **2018**, *30*, e1706654. [CrossRef] [PubMed]

16. Deklerck, V.; De Mil, T.; Kondjo, P.; Beeckman, H.; Van Acker, J.; Bulcke, J.V.D. Sleeping beauties in materials science: Unlocking the value of xylarium specimens in the search for timbers of the future. *Holzforschung* **2019**, *73*, 889–897. [CrossRef]
17. Yi, Q.; Li, J.; Zhang, R.; Ma, E.; Liu, R. Preparation of small particle diameter thermally expandable microspheres under atmospheric pressure for potential utilization in wood. *J. Appl. Polym. Sci.* **2021**, *138*, e49734. [CrossRef]
18. Borrega, M.; Ahvenainen, P.; Serimaa, R.; Gibson, L. Composition and structure of balsa (*Ochroma pyramidale*) wood. *Wood Sci. Technol.* **2015**, *49*, 403–420. [CrossRef]
19. de Almeida Varasquim, F.M.F.; de Sampaio Alves, M.C.; Gonçalves, M.T.T.; Santiago, L.F.F.; de Souza, A.J.D. Influence of belt speed, grit sizes and pressure on the sanding of Eucalyptus grandis wood. *Cerne* **2012**, *18*, 231–237. [CrossRef]
20. Liu, Y.; Hu, J.; Xu, W. Surface Roughness of wood substrates after grinding and its influence on the modification effect of structural color layers. *Forests* **2023**, *14*, 2213. [CrossRef]
21. Hu, J.; Liu, Y.; Xu, W.; Wu, Z.; Pang, X. Construction of rainbow-like structural color coatings on wood surfaces based on polystyrene microspheres. *Forests* **2023**, *14*, 76. [CrossRef]
22. Cataldi, A.; Corcione, C.E.; Frigione, M.; Pegoretti, A. Photocurable resin/nanocellulose composite coatings for wood protection. *Prog. Org. Coat.* **2017**, *106*, 128–136. [CrossRef]
23. Li, Y.; Li, J. Fabrication of reversible thermoresponsive thin films on wood surfaces with hydrophobic performance. *Prog. Org. Coat.* **2018**, *119*, 15–22. [CrossRef]
24. Vogel, N.; Retsch, M.; Fustin, C.-A.; del Campo, A.; Jonas, U. Advances in colloidal assembly: The design of structure and hierarchy in two and three dimensions. *Chem. Rev.* **2015**, *115*, 6265–6311. [CrossRef]
25. Zhou, L.; Li, Y.; Liu, G.; Fan, Q.; Shao, J. Study on the correlations between the structural colors of photonic crystals and the base colors of textile fabric substrates. *Dye. Pigment.* **2016**, *133*, 435–444. [CrossRef]
26. Spicer, R. Symplasmic networks in secondary vascular tissues: Parenchyma distribution and activity supporting long-distance transport. *J. Exp. Bot.* **2014**, *65*, 1829–1848. [CrossRef]
27. Wang, F.; Guo, F.; Xue, Y.; Luo, H.; Zhu, J. Rapid fabrication of large-scale structurally colored PS@SiO_2 films with enhanced self-cleaning capability. *J. Coat. Technol. Res.* **2021**, *18*, 489–499. [CrossRef]
28. Li, Y.; Fan, Q.; Wang, X.; Liu, G.; Chai, L.; Zhou, L.; Shao, J.; Yin, Y. Shear-induced assembly of liquid colloidal crystals for large-scale structural coloration of textiles. *Adv. Funct. Mater.* **2021**, *31*, 2010746. [CrossRef]
29. Suh, Y.; Gowda, H.; Won, Y. In situ investigation of particle clustering dynamics in colloidal assemblies using fluorescence microscopy. *J. Colloid Interface Sci.* **2020**, *576*, 195–202. [CrossRef] [PubMed]
30. Huang, Y.; Zhou, J.; Su, B.; Shi, L.; Wang, J.; Chen, S.; Wang, L.; Zi, J.; Song, Y.; Jiang, L. Colloidal photonic crystals with narrow stopbands assembled from low-adhesive superhydrophobic substrates. *J. Am. Chem. Soc.* **2012**, *134*, 17053–17058. [CrossRef] [PubMed]
31. Suh, Y.; Pham, Q.; Shao, B.; Won, Y. The control of colloidal grain boundaries through evaporative vertical self-assembly. *Small* **2019**, *15*, e1804523. [CrossRef]
32. Li, B.; Jiang, B.; Han, W.; He, M.; Li, X.; Wang, W.; Hong, S.W.; Byun, M.; Lin, S.; Lin, Z. Harnessing colloidal crack formation by flow-enabled self-assembly. *Angew. Chem. Int. Ed.* **2017**, *56*, 4554–4559. [CrossRef]
33. Qin, Z.; Gao, Q.; Zhang, S.; Li, J. Surface free energy and dynamic wettability of differently machined poplar woods. *BioResources* **2014**, *9*, 3088–3103. [CrossRef]

Disclaimer/Publisher's Note: The statements, opinions and data contained in all publications are solely those of the individual author(s) and contributor(s) and not of MDPI and/or the editor(s). MDPI and/or the editor(s) disclaim responsibility for any injury to people or property resulting from any ideas, methods, instructions or products referred to in the content.